EÖTVÖS LORÁND UNIVERSITY

FACULTY OF SCIENCE

DEPARTMENT OF MATERIALS SCIENCE

Numerical simulation of silicon quantum dots

Supervisor:
Dr. Széchenyi Gábor
Assistant Professor

Author:
Nur Atikah Tadjuddin
Materials Science MSc

Budapest, June 2022

Contents

Chapter 1

Introduction

The idea of quantum computing was first proposed in the 1980s when it was proposed to build computers based on the laws of quantum physics instead of classical physics [1]. However, this approach requires the challenge of assembling and controlling quantum systems where typically it only appears at the level of fundamental matter, such as atoms and electrons. Over the past decades, there has been seemingly rapid progress in addressing this challenge and how to make quantum system become accessible and open up a new level of computational possibilities to solve problems that relatively need large computational time for classical computers [2]. For instance, Grover's algorithm [3] to search for an element in an unstructured list, Shor's algorithm [4] for prime factorization, and efficient simulation of quantum many-body systems.

Quantum computer and classical computer use different basic units of data. In classical computing, information is encoded in bits (1s and 0s), while quantum computing uses qubits. A single bit can deliver an outcome that is either 1 or 0. On the other hand, the value of a qubit can be 0, 1, or any superposition of both states. Hence, a qubit can take on various values at one time and perform calculations beyond a classical computer. However, during these operations the quantum system needs to be protected against the noise to avoid the loss of quantum superposition.

There are several platforms that can be used for qubits including semiconductor quantum dots [5], trapped ions [6], superconducting circuits [7], photonic systems [8], etc. The current state of trapped-ion and superconducting qubit platforms boasts a higher number of qubits controlled in a system compared to the semiconductor spin platform. The trapped-ion platform can hold up to 32 ion qubits [9] and a

superconducting platform with 127 qubits [10]. The latter was the Eagle processor launched by IBM, surpassing the previous Google's Sycamore chip with 53 qubits. On the contrary, the semiconductor spin platform only has four qubits [11]. However, semiconductor qubits provide an advantage in their small footprint and scalability.

Quantum dots can be referred to as artificial atoms. This is due to their discrete energy levels as in the real atoms when the electrons are confined in all three spatial directions [12–14]. Quantum dots can exist in a variety of sizes and materials since it is a general kind of system. For instance, self-assembled quantum dots, single molecules trapped between electrodes, and quantum dots in a semiconductor using confining potential. Quantum dots can also come in various shapes, such as in quasi one-dimensional objects like nanotubes or nanowires and two-dimensional objects like thin films, two-dimensional electron gas, or quantum wells. There are many ways to fabricate quantum dots. One of them is lithographic fabrication. Tiny gate electrodes were placed on the top of a layer of semiconductor heterostructure that confines electrons in two dimensions. These electrodes were fabricated by using electron-beam lithography. Negative voltages can be applied to the gates, resulting in the confinement of electrons into one and small islands. These quantum-confined islands are the quantum dots [16]. The schematic figure of quantum dots with a tunable number of electrons fabricated from a GaAs/AlGaAs two-dimensional electron gas (2DEG) is shown in Figure 1.1a. The confinement in the horizontal axis is achieved by electric fields through metallic surface gates above the 2DEG, and confinement in the vertical axis is due to the boundary of GaAs/AlGaAs. In addition, Figure 1.1b shows a scanning electron micrograph image of a few-electron single-dot device.

For over the last twenty years, many research has been conducted on qubits that are based on the freedom of electrons in quantum dots. For instance, the electron's charge, spin, and valley states. A natural choice for the qubit is the electron spin, where the spin-up corresponds to $|1\rangle$ state and the spin-down with $|0\rangle$ state. Spin qubits in semiconductors, like silicon, germanium, or gallium arsenide, can be used for scalable quantum computing schemes. To represent a qubit by electron spins, individual electrons can be electrostatically trapped in a heterostructure material, such as silicon-germanium (SiGe). Figure 1.2a shows a scanning electron microscopy image of a Si/SiGe heterostructure. The two circles represent the two spin qubits in the double dots. Furthermore, Figure 1.2b shows a schematic image of the two elec-

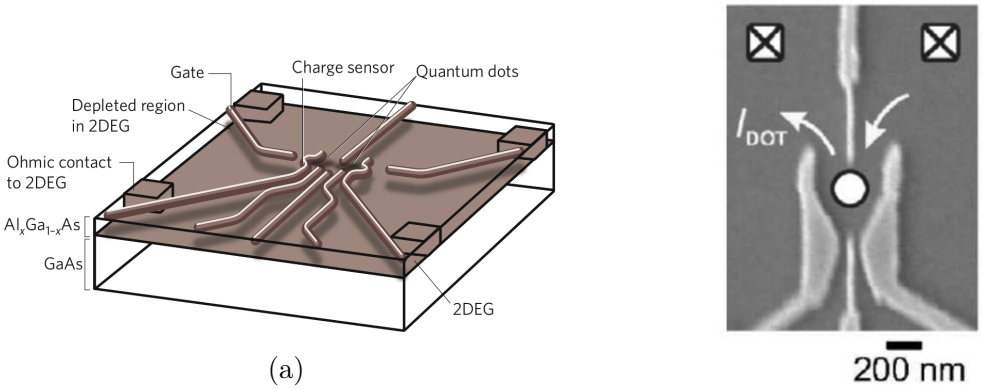

(a) (b)

Figure 1.1: (a) A schematic view of a quantum dot defined in a two-dimensional electron gas [15]. (b) Scanning electron micrograph of the single quantum dot device [16].

tron trap sample that formed the double quantum dots in Si/SiGe heterostructure.

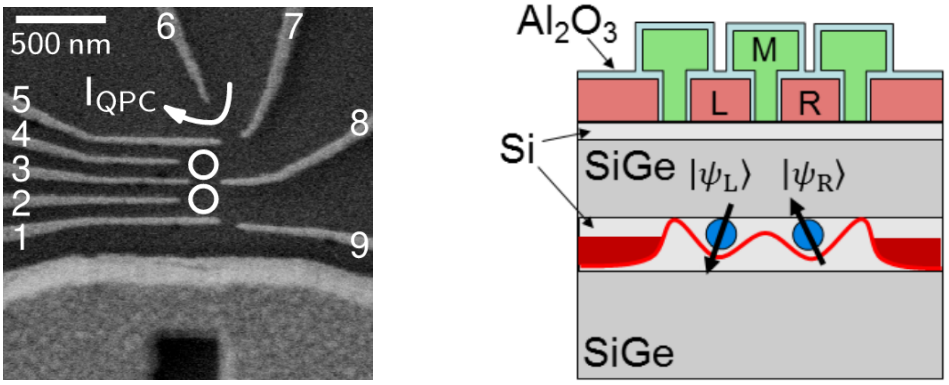

(a) (b)

Figure 1.2: (a) A SEM image of the quantum dots device that fabricated on a Si/SiGe heterostructures [17]. (b) A schematic cross-sectional view of the double quantum dots. Two electrons are trapped in the confinement potential created by gates L, M, and R, with an aluminum oxide (Al_2O_3) layer between each gate [18].

As mentioned before, there are several candidates for using the degree of freedom of electrons as qubits. Besides the electron's spin and charge, we can also use valley states. Valleys are the minima in the electronic band structure (conduction band) [19]. An electron can occupy one of these valleys, and the valley can be considered as an additional degree of freedom for the particle besides spin and charge. Some materials possess multiple degenerate valleys in their conduction band. For instance, graphene with its two-fold valley degeneracy [20], bulk aluminum arsenide (AlAs) with three degenerate valleys in its conduction band [21], and silicon which has six degenerate valleys. The latter is what we would like to focus on in this work.

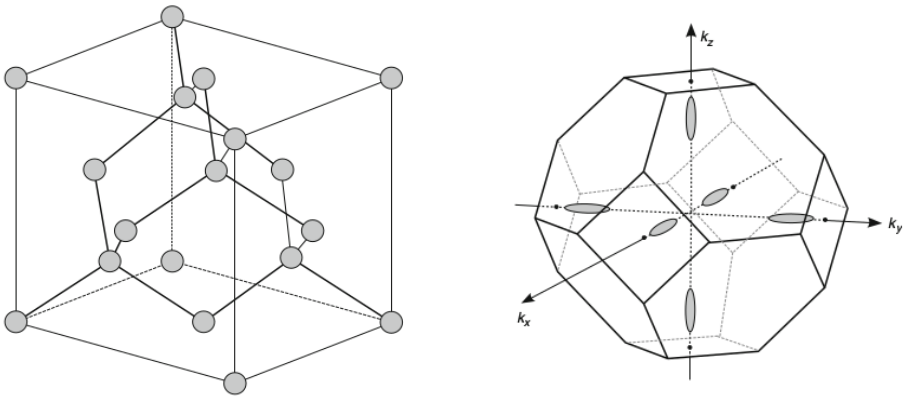

(a) (b)

Figure 1.3: (a) Crystal structure of silicon. (b) First Brillouin zone of silicon crystal lattice. [22]

The properties of silicon are very interesting for quantum computing. The crystal structure of silicon is a diamond structure, as shown in Figure 1.3a. The crystal lattice can be represented as two face-centered cubic lattices (fcc), where the second lattice of atoms B is shifted relative to the first one of atoms A by a translation vector along a diagonal. In the case of silicon, both atoms are identical. This is also the case for typical semiconductors of group IV. It is shown in fig. 1.3b, the six equivalent valleys of the conduction band of silicon along the three principal axes. Hence, the bulk silicon has six degenerate valleys in its conduction band, and the energies of the six states are the same due to the symmetry.

In the presence of confinement potential, the system can exhibit intriguing phenomena. The symmetry is broken, and the degeneracy is lifted. Other effects such as strain and electric fields can also cause this six-fold degeneracy in bulk silicon to be broken. In this case, we will have four-fold degeneracy with high energy and two-fold degeneracy with low energy (Fig 1.4). These lowest two states are not completely degenerate because there is a small energy gap between the states, which is referred to as valley splitting. It is crucial to calculate this valley splitting because this is the qubit splitting in our model where the ground state corresponds to $|0\rangle$ state and the first excited state corresponds to $|1\rangle$ state, and it needs to be under control. Otherwise, if this splitting is not constant, it can be a noise factor in our model resulting in decoherence and dephasing where the phase information of the qubit is lost.

In this work, we aim to model this valley splitting in a silicon quantum dot with a one-dimensional tight-binding model and calculate its value. We also investigate

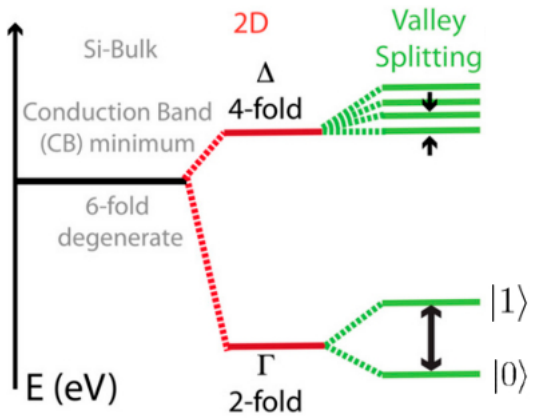

Figure 1.4: The six-fold valley degeneracy of bulk silicon is broken into four-fold and two-fold degeneracy. The two-fold degeneracy is broken by the confinement potential [23].

how this valley splitting changes when we modify the confinement potential.

1.1 Motivation

Qubits as the basic unit in quantum computer can be constructed from several physical systems with distinct quantum states, such as the polarization of a photon, the spin degree of freedom, charge freedom, and the valley freedom of an electron, and so on. In this case, we would like to make qubits in silicon by considering the valley freedom of an electron in silicon. There are several points why silicon is an interesting platform for quantum computers.

1. Silicon is a well-known material in the semiconductor industry. Due to its abundance, intrinsic properties, and the ease in its fabrication, many electronic and optical devices such as transistors, integrated circuits, and processors are based on silicon. Based on this, it is possible to manufacture qubits in silicon at a low cost.

2. Silicon is a spinless material, which means that it has low spin-orbit coupling. Natural silicon has approximately a 4.7% concentration of ^{29}Si isotopes, which contain a non-zero nuclear spin. Whereas the two naturally abundant isotopes, ^{28}Si and ^{30}Si, are spinless. Spin is a potential source of noise and decoherence [24]. Therefore, these properties contribute to long spin coherence times [25].

3. Silicon-based qubits have a relatively small size compared to the other types of qubits. For instance, state-of-the-art quantum computers using trapped ions

and superconducting qubits have a typical size of a few millimeters area that is needed for one qubit [7, 26]. In comparison, silicon-based qubits are much smaller in the nanoscale regime [27].

As we mentioned before, in this case we would like to work on silicon-based qubits that use the valley freedom. There are several reasons why it is interesting to use the valley freedom as qubits.

1. Valley qubit in a silicon quantum dot has protection against the charge and magnetic noise [28, 29]. In quantum computing, it is essential to maintain the coherent superposition of quantum states from any disturbance such as the noise from an environment that can lead to decoherence and the loss of qubit information. In the case of valley freedom, its electron density for the two states, the ground state and the first excited state, has the same envelope function. This means that if we have some potential fluctuations in the system, the two energy levels are shifted with the same value. Therefore, the qubit splitting remains the same, and it does not give any contribution to the noise or decoherence.

2. Valley splitting in a silicon quantum dot can be controlled electrostatically in the range from 0.3 to 0.8 meV [30]. Electrical manipulation is a fundamental condition to ensure coherent valley operations.

Chapter 2

Tight-binding model

2.1 Tight-binding model for electrons in 1D

To calculate the valley splitting in a silicon quantum dot, we would like to use a one-dimensional tight-binding model when we have a 1D crystal. This section presents our review of this tight-binding model and the calculation to obtain the dispersion relation.

The band structure calculation can be done in several approaches. One of the commonly used techniques is the tight-binding model. This model involves electrons that are bound to atomic orbitals at each site of the crystal lattice and allows the hopping of electrons between the neighboring sites, as shown schematically in the Figure 2.1. In this approximation, the long-range hopping can be neglected because its amplitude is small due to the exponential decay as distance increases.

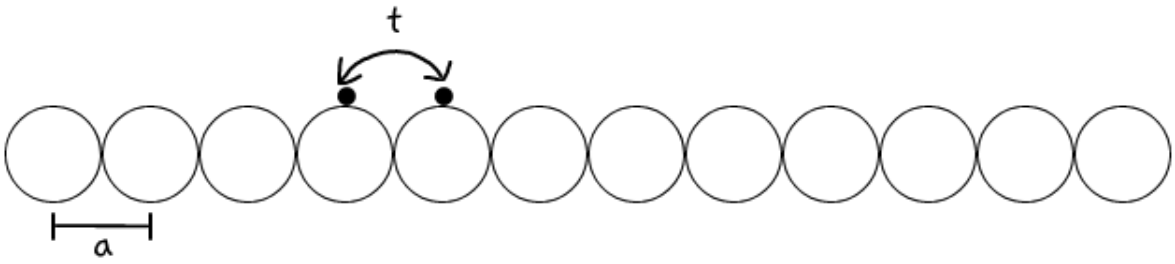

Figure 2.1: Schematic illustration of one dimensional tight-binding model with hopping parameter t and atomic distance a.

In many-body system, the tight-binding Hamiltonian can be written in a second quantized form, as expressed in Equation 2.1

$$H = \varepsilon_0 \sum_{i,\sigma} c_{i\sigma}^{\dagger} c_{i\sigma} - t \sum_{\langle ij \rangle,\sigma} \left(c_{i\sigma}^{\dagger} c_{j\sigma} + h.c. \right) \tag{2.1}$$

where the t is the hopping parameter, ε_0 is the onsite energy term, $\langle ij \rangle$ indicates the site indices and they are neighbors, σ is the spin polarization, and $c_{i\sigma}^{\dagger}$ and $c_{j\sigma}$ are creation and annihilation operators. The $c_{i\sigma}^{\dagger}$ is defined as the operator that creates one electron with spin σ at site i. Likewise, the $c_{j\sigma}$ annihilates an electron with spin σ at site j. However, in this work, we neglect this spin freedom because we will focus on the spinless model. The $h.c.$ term means the hermitian conjugate of the other term, which in this case $c_{j\sigma}^{\dagger} c_{i\sigma}$.

In the tight-binding model, several assumptions are made. We begin with the assumption that all the orbitals are orthogonal. Then, we identify the basis states where we have one orbital for each atom. We can express this by Eq. 2.2, and label the orbital for the electron at atom n as $|n\rangle$.

$$\langle n|m\rangle = \delta_{n,m} \tag{2.2}$$

where $\delta_{n,m}$ is the Kronecker delta.

$$\delta_{n,m} = \begin{cases} 1, & \text{if } n = m, \\ 0, & \text{if } n \neq m. \end{cases} \tag{2.3}$$

The general form of the wave functions that can be a solution to the Hamiltonian is a superposition of these orbital states which means that the electron can be split between these orbital states. We will look for solutions to our model on the basis of atomic orbitals. Therefore, a one-dimensional tight-binding model is known as the LCAO (linear combinations of atomic orbitals) method. The state and the wave function of the electron in the basis of the orbitals can be written in Eq. 2.4. In addition, the time-independent Schrödinger equation on the basis of orbitals reads as Eq. 2.5.

$$|\psi\rangle = \sum_{n} d_n |n\rangle \tag{2.4}$$

$$H|\psi\rangle = E|\psi\rangle \tag{2.5}$$

Alternatively, we can write the Eq.2.5 in the form of a component matrix multiplication as follows

$$\sum_m H_{nm} d_m = E d_n \tag{2.6}$$

with $H_{nm} = \langle n|H|m\rangle$ as the matrix elements.

Since the Hamiltonian only couples the nearest neighbor sites, so we can write an approximation as

$$\langle n|H|m\rangle = \begin{cases} \varepsilon_0, & \text{for } n = m \\ -t, & \text{for } n = m \pm 1 \\ 0, & \text{otherwise.} \end{cases} \tag{2.7}$$

The ε_0 term denotes the on-site energy or the atomic orbital energy, and in this case it is constant at each site. The t parameter is the tunnelling term. When the difference between n and m is bigger than one, then we neglect this term of $\langle n|H|m\rangle$ because it will be relatively smaller than ε_0 and t parameters.

$$\sum_m H_{nm} d_m = E d_n \tag{2.8}$$

$$\sum_m \varepsilon_0 d_m - t \sum_m \delta_{n,m+1} + \delta_{n,m} - 1 d_m = E d_n \tag{2.9}$$

$$\varepsilon_0 d_n - t(d_{n-1} + d_{n+1}) = E d_n \tag{2.10}$$

Fourier Transformation The tight-binding Hamiltonian, as expressed in Eq. 2.1, is not diagonal since it contains two different operators. To solve the Hamiltonian, we need to do a Fourier transform to diagonalize it by changing the basis.

According to the Bloch theorem, the solution of the Schrödinger wave equation for an electron moves in a periodic potential is of the form of some periodic function times a plane wave. We use the following ansatz form

$$d_n = \frac{e^{ikna}}{\sqrt{N}} \tag{2.11}$$

From this, we substitute the d_n into the Eq. 2.10 as follows

$$\varepsilon_0 \frac{e^{ikna}}{\sqrt{N}} - t\left(\frac{e^{-ik(n-1)a}}{\sqrt{N}} + \frac{e^{-ik(n+1)a}}{\sqrt{N}}\right) = E\frac{e^{-ikna}}{\sqrt{N}}$$
$$\frac{e^{-ikna}}{\sqrt{N}}\left(\varepsilon_0 - t\left(e^{ika} + e^{-ika}\right)\right) = E\frac{e^{-ikna}}{\sqrt{N}}$$
$$\varepsilon_0 - t\left(2\cos ka\right) = E$$

Then we can obtain the dispersion relation for the one-dimensional tight-binding model as the following,

$$E(k) = \varepsilon_0 - 2t\cos ka \tag{2.12}$$

A plot of this energy dispersion relation is shown in Figure 2.2.

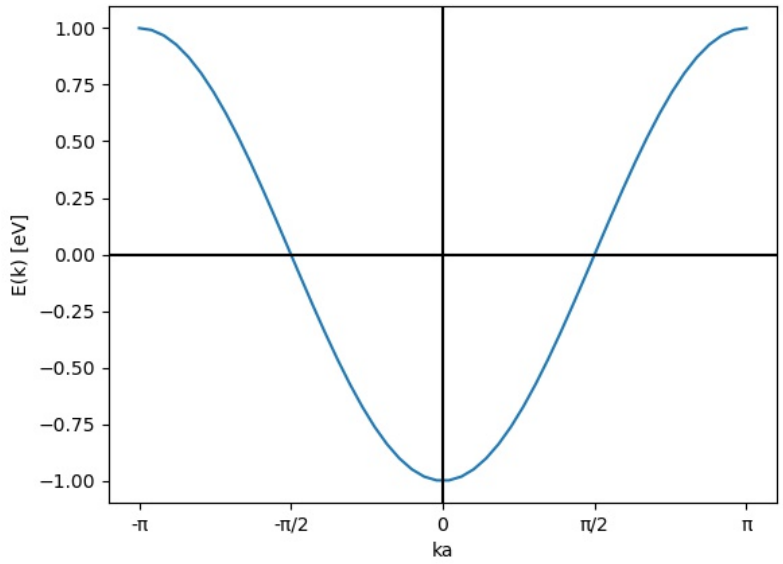

Figure 2.2: Dispersion relation of the one-dimensional tight-binding model, according to 2.12, where $\varepsilon_0 = 0$ eV and $t = 0.5$ eV.

2.2 Tight-binding model for silicon

In this section, we would like to modify the previous model to describe the valley feature of the silicon. This is the simplest possible model for the conduction band of Si that can accurately reproduce the lowest conduction band of silicon in 1D. The tight-binding Hamiltonian for silicon in a real-space representation reads as Eq. 2.13,

$$H = \sum_i \varepsilon_i c_i^\dagger c_i - t_1 \sum_i \left(c_{i+1}^\dagger c_i + h.c. \right) - t_2 \sum_i \left(c_{i+2}^\dagger c_i + h.c. \right) \tag{2.13}$$

In this model, we have an additional parameter where we take into account for not only the interaction with the next neighbor but also with the next nearest neighbor sites, where each is represented by the hopping terms, t_1 and t_2. ε_i is the onsite energy that depends on the i as the site index. In this Hamiltonian, we omit the spin term (σ) since we will focus on the spinless model. After we fit all these parameters, we would obtain the dispersion relation and check the effective mass and position of the minima.

To obtain the dispersion relation, first, we can re-write the approximation for the matrix elements in the Hamiltonian as Eq. 2.14. Here we focus on the homogeneous model when ε is constant ($\varepsilon_i = \varepsilon_0$).

$$\langle n|H|m\rangle = \begin{cases} \varepsilon_0, & \text{for } n = m \\ t_1, & \text{for } n = m \pm 1 \\ t_2, & \text{for } n = m \pm 2 \\ 0, & \text{otherwise} \end{cases} \tag{2.14}$$

Then we substitute these parameters into the Eq. 2.6.

$$\sum_m \varepsilon_0 \delta_{n,m} d_m + t_1 \sum_m \left(\delta_{n,m+1} + \delta_{n,m-1} \right) d_m + t_2 \sum_m \left(\delta_{n,m+2} + \delta_{n,m-2} \right) d_m = E d_n$$
$$\varepsilon_0 d_n + t_1 \left(c_{n-1} + c_{n+1} \right) + t_2 \left(c_{n-2} + c_{n+2} \right) = E d_n$$

In this case, we use an ansatz

$$d_n = \frac{e^{ikna}}{\sqrt{N}} \tag{2.15}$$

$$\varepsilon_0 \frac{e^{-ikna}}{\sqrt{N}} + t_1 \left(\frac{e^{-ik(n-1)a}}{\sqrt{N}} + \frac{e^{-ik(n+1)a}}{\sqrt{N}} \right) + t_2 \left(\frac{e^{-ik(n-2)a}}{\sqrt{N}} + \frac{e^{-ik(n+2)a}}{\sqrt{N}} \right) = E d_n$$
$$\frac{e^{-ikna}}{\sqrt{N}} \left(\varepsilon_0 + t_1 \left(e^{ika} + e^{-ika} \right) + t_2 \left(e^{i2ka} + e^{-i2ka} \right) \right) = E \frac{e^{-ikna}}{\sqrt{N}}$$
$$\varepsilon_0 + t_1 \left(2 \cos ka \right) + t_2 \left(2 \cos 2ka \right) = E$$
$$E = \varepsilon_0 + 2t_1 \cos ka + 2t_2 \cos 2ka$$

We obtain the dispersion relation for this model

$$E(k) = \varepsilon_0 + 2t_1 \cos ka + 2t_2 \cos 2ka \tag{2.16}$$

A plot of this energy dispersion relation is shown in Figure 2.3.

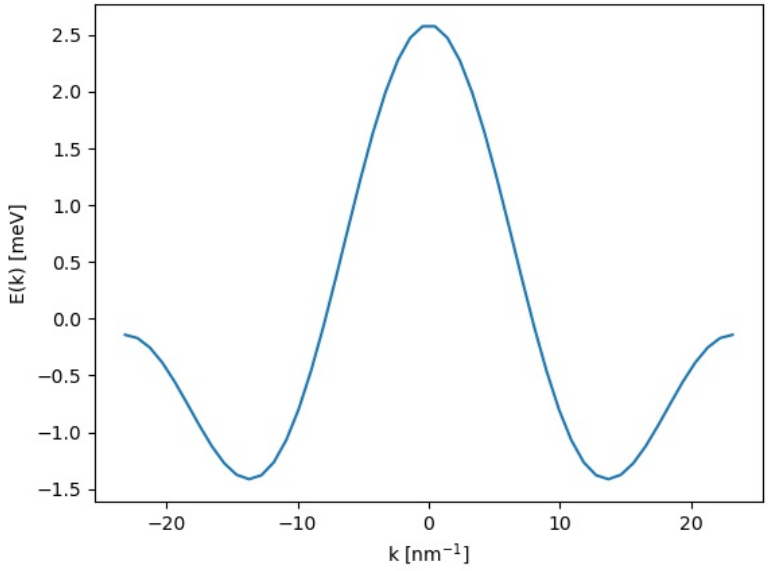

Figure 2.3: Dispersion relation.

Figure 2.3 shows the dispersion relation which is different from the previous model where it only has one minimum point at the middle (Fig. 2.2). In this case, we have two minima and these are the valleys. According to this result, this model is good for materials that have two valleys. In our work, we will use these valleys as a qubit.

From the silicon band structure, we get two values, the position of the minima (k_0) and the effective mass (m_e). We would like to find the corresponding t_1 and t_2 values which give the correct values for the k_0 and m_e. The lattice constant a, which defines the spacing between the silicon atoms, is given. It is divided by four which come from the crystal structure of the silicon. According to Boykin et al. [31], the values for each parameter are the following,

$$t_1 = 683 \text{ meV} \tag{2.17}$$

$$t_2 = 612 \text{ meV} \tag{2.18}$$

$$a = \frac{0.543}{4} \text{ nm} \tag{2.19}$$

From this, we we can check the position of the minima as the k_0 value, by substituting parameters value of t_1, t_2, and a (lattice constant) into the equation below

$$\frac{\partial E(k)}{\partial k} = 0 \tag{2.20}$$

$$\begin{aligned} -2t_1 a \sin ka - 4t_2 a \sin 2ka &= 0 \\ -t_1 \sin ka &= 2t_2 \sin 2ka \\ -t_1 \sin ka &= 4t_2 \sin ka \cos ka \\ -\frac{t_1}{4t_2} &= \cos k_0 a \\ k_0 = 13,65 \text{ nm}^{-1} & \end{aligned}$$

and we obtain that k_0 is 13,65 nm^{-1}, which is the correct value for silicon.

Effective mass The effective mass is an important parameter when the electron is moving within a solid material in a periodic potential. We can find the effective mass by evaluating the region around k_0 by doing Taylor expansion and approximate the polynomials near some input, which is $k_0 + \Delta k$.

$$\epsilon(k) = \epsilon(k_0) + (k - k_0) \left[\epsilon'(k)\right]_{k=k_0} + \frac{1}{2}(k - k_0)^2 \left[\epsilon''(k)\right]_{k=k_0} \tag{2.21}$$

Since $\epsilon'(k)$ indicate the gradient at $k = k_0$, the value of this term is zero.

$$\begin{aligned} \epsilon(k) &= \epsilon(k_0) + \frac{1}{2}(k - k_0)^2 \left[\epsilon''(k)\right]_{k=k_0} \\ \frac{1}{2}(k - k_0)^2 \left[\epsilon''(k)\right]_{k=k_0} &= \frac{\hbar^2}{2m_e}(k - k_0)^2 \end{aligned}$$

$$m_e = \frac{\hbar^2}{\left[\epsilon''(k)\right]_{k=k_0}} \tag{2.22}$$

To find the effective mass, based on eq. 2.22, first we will look for $\epsilon''(k)$, and substitute the value.

$$\begin{aligned}
\epsilon''(k) &= -2t_1a^2\cos ka - 8t_2a^2\cos 2ka \\
[\epsilon''(k)]_{k=k_0} &= -2t_1a^2\cos k_0a - 8t_2a^2\left(2\cos^2 k_0a - 1\right) \\
[\epsilon''(k)]_{k=k_0} &= -2t_1a^2\left(-\frac{t_1}{4t_2}\right) - 8t_2a^2\left(\frac{t_1^2}{8t_2^2} - 1\right) \\
[\epsilon''(k)]_{k=k_0} &= -\frac{1}{2}\frac{a^2t_1^2}{t_2} + 8a^2t_2 \\
[\epsilon''(k)]_{k=k_0} &= 83.2\ \mathrm{nm^2meV}
\end{aligned}$$

From this, the effective mass is

$$m_e = 8.35 \times 10^{-31}\ \mathrm{kg} = 0.916m_0 \tag{2.23}$$

This value gives the correct longitudinal effective mass for silicon according to Hensel *et al.* [32]

Chapter 3

Confinement Potential

In this part, we would like to investigate what happens with these valleys when we have a confining potential. In the presence of confinement potential, the degeneracy is lifted, and we would like to calculate the valley splitting between the two lowest energy states. However, before we apply this confinement to the tight-binding model, first we analyze the well-known problem where we have a free electron in the quantum well. We would like to solve this continuous model with the Schrödinger equation. Hence in the first part, we will focus on the infinite potential well and in the second part we will focus on the tight-binding model.

3.1 Free electron model

The infinite potential well is one of the toy models of a quantum well system. It is also known as the particle in a box model. It describes how a free particle moves in a box with impenetrable walls that can be modeled by the potential given in Eq. 3.1. As shown in Fig. 3.1, there are hard walls that prevent the particle from going to $x > L$ and $x < 0$. So we can expect that the wavefunction must have vanished when the potential is infinite. L here is the length of the well. The potential is defined as

$$V(x) = \begin{cases} 0, & 0 < x < L, \\ \infty, & x \leq 0, x \geq L \end{cases} \tag{3.1}$$

In the case of a flat model without any confinement, the onsite energy term is constant throughout every site. However, when we turn on the confinement potential which is the infinite quantum well, the potential is zero inside the quantum well and becomes infinitely large outside the range L. We can impose the potential into the

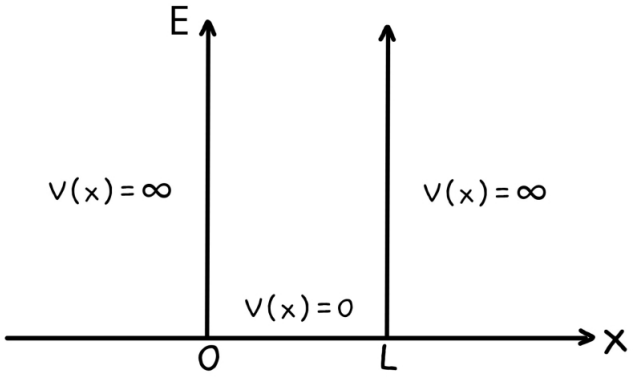

Figure 3.1: Infinite square well potential.

continuous model by using the time-independent form of the Schrödinger equation as expressed in Eq. 3.2

$$H\psi(x) = E\psi(x) \tag{3.2}$$

$$H = \frac{\hbar^2}{2m}\frac{d^2}{dx^2} + V(x) \tag{3.3}$$

According to Eq. 3.1, when the potential $V(x) = \infty$, we must expect that the wavefunction is vanished, i.e. $\psi(x) = 0$, and the probabiltiy is zero. However, when $V(x) = 0$, we can calculate the wavefunction using the Eq. 3.2. A solution to this wavefunction can be written as,

$$\psi(x) = \begin{cases} \sqrt{\frac{2}{L}} \sin\left(\frac{n\pi x}{L}\right), & \text{where } n = 1, 2, 3, ... \text{ and } 0 < x < L, \\ 0, & \text{otherwise.} \end{cases} \tag{3.4}$$

The wave function in quantum mechanics can be used to illustrate the wave properties of a particle. However, the function itself has no physical meaning as it is not a quantity that can be observed. Nevertheless, if we take the square of the absolute value of the wave function ($|\psi|^2$), it will give important information. The amplitude of the wavefunction at a given position is related to the probability of finding a particle in a certain region by $P(x,t) = |\psi(x,t)|^2$.

3.2 The tight-binding model

The setup used in this work is when we have an electron in silicon treated with a tight-binding model in the infinite square well potential. We work on Eq. 2.13, where $\varepsilon_i = 0$ when $0 < i < L$. Here, L denotes the number of sites in our model and we choose to work on 100 sites. Using the eigenvalues and eigenvectors obtained by exact diagonalization of the Hamiltonian matrix of our model, we can calculate the probability densities. Then, we plot the probability density function, and obtained the result as seen in Fig. 3.2, 3.3, and 3.4 for the ground state, the first excited state, and the second excited state. To explain this behavior, it is worth noting that for a particle in a box model, the wave function is a sine function [33]. We observed that the envelope function for the probability density figures of the $|0\rangle$ and the $|1\rangle$ states is the same as the probability density function for the ground state of a free electron in an infinite quantum well. We also noticed a fast oscillation because we have an additional minimum in the conduction band (k_0) as shown in Fig. 2.3. These two states represent the two valley states which are used as a qubit. Moreover, for the second excited state (Fig. 3.4), it exhibits the same envelope function as the higher state in a simple model.

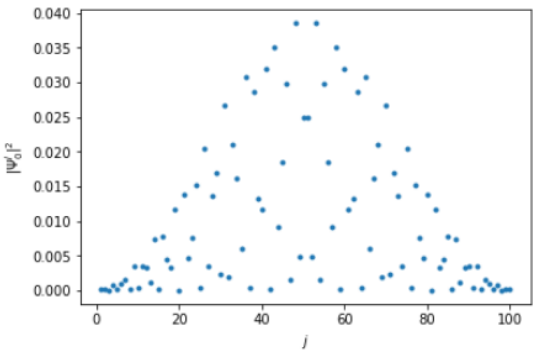

Figure 3.2: $|0\rangle$ state

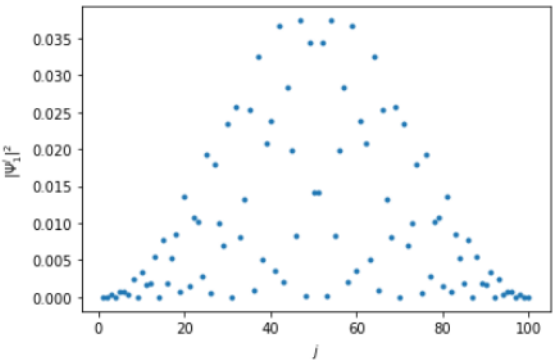

Figure 3.3: $|1\rangle$ state

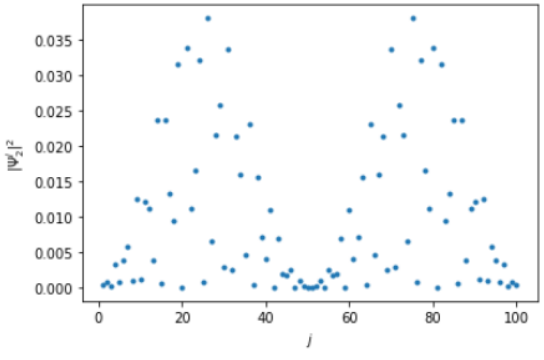

Figure 3.4: Second excited state

3.3 Valley splitting in infinite square well potential

Qubit is the fundamental unit of quantum information. It can be constructed from an object that can obtain a quantum superposition between two states. A spin of an electron is one of the examples where we can treat the spin up and spin down as two states, the $|1\rangle$ and $|0\rangle$ states, respectively. Another example is a polarization of a photon, where the two states can be taken to be the vertical polarization and the horizontal polarization.

In quantum computing, the presence of degeneracy can be a source of decoherence, and it can degrade the computation. Multiple minimums or valleys in the silicon conduction band can threaten the qubit operation. Hence, we need to lift this valley degeneracy by creating a valley splitting.

Since we will use the valley states as a qubit, it is crucial to find the size of the valley splitting. To calculate the valley splitting, we can use the exact diagonalization method of the Hamiltonian matrix from our tight-binding model and obtain the low energy eigenstates and the corresponding eigenvalue. As mentioned before, the same envelope function between the two lowest states renders the protection against charge noise. Fig. 3.5 shows the valley splitting between the two lowest states denoted by ΔE as a function of the number of sites in the square well potential denoted by L. In our numerical calculation, we observe an oscillation and a decaying trend. We can see that the energy splitting decreases as the length increases. This was also investigated analytically in the literature [31], which also gives the formula for the valley splitting.

We present two results, the numerical simulation, and the analytical calculation. Here we attempt to produce the well-known result from the literature (Boykin et al. [31]). Results of our numerical simulation are compared with the analytical calculation from the paper. By this, we try to verify our method and simulation codes.

Analytical calculation According to Boykin *et al.* [31], the analytical formulas for the valley splitting were derived. They used the same tight-binding model to calculate the valley splitting. The result is expressed as the following,

$$\Delta E = |E_1 - E_0| \approx \frac{16\pi^2 t_2}{(L+2)^3} \sin\left(\frac{\Phi_{\min}}{2}\right) \left|\sin\left[(L+2)\frac{\Phi_{min}}{2}\right]\right| \tag{3.5}$$

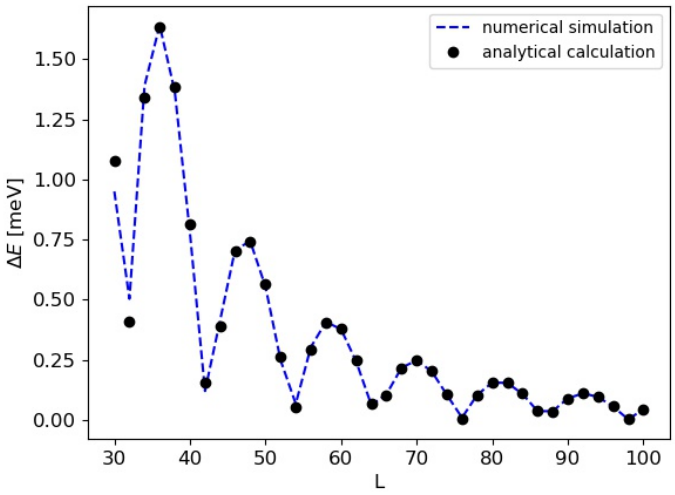

Figure 3.5: Valley splitting

where L is the length of the system and the two-band phase Φ_{min} can be calculated via the one-band phase ρ_{min}, where $\rho_{min} = \pi - \frac{\Phi_{min}}{2}$ and $\cos(\rho_{min}) = -t_1/4t_2$. t_1 and t_2 are the nearest-neighbor and second-nearest-neighbor parameters, respectively.

3.4 Parabolic confinement

3.4.1 Valley splitting

In this part, we would like to investigate another type of confinement. We introduce the parabolic confinement and calculate the valley splitting between the two lowest energy states. The parabolic confinement can be modeled as a harmonic potential at a stable equilibrium position in which the onsite energy increases as we go further from the middle point of the confinement potential. The potential is varied as a function of the onsite energy term that depends on the site index. It can be expressed as Eq. 3.6 below,

$$\varepsilon_i = Ai^2 \tag{3.6}$$

where A indicate the strength of the confinement and i is the site index.

In Fig. 3.6, the valley splitting ΔE is plotted as a function of the strength of the confinement indicated by the A value. The larger the A value, the sharper the parabolic confinement is. Furthermore, by this, if we have a small A value, that

means the effect of this parabolic confinement is weaker, and when we increase this A value, we will find how this effect of parabolic confinement becomes more important than the square-well potential. This calculation is based on our model, which contains 100 sites. The number of sites is due to our observation that the effect of parabolic confinement becomes more pronounced when we increase the length of the system.

When we set the strength of the parabolic confinement between 1-50, the valley splitting is on the same order of magnitude as in the case of a quantum well. However, the valley splitting increases significantly as we set the A higher and eventually, we reached the order of 10 meV as we set it to 100, which means the sharpest parabolic in this model.

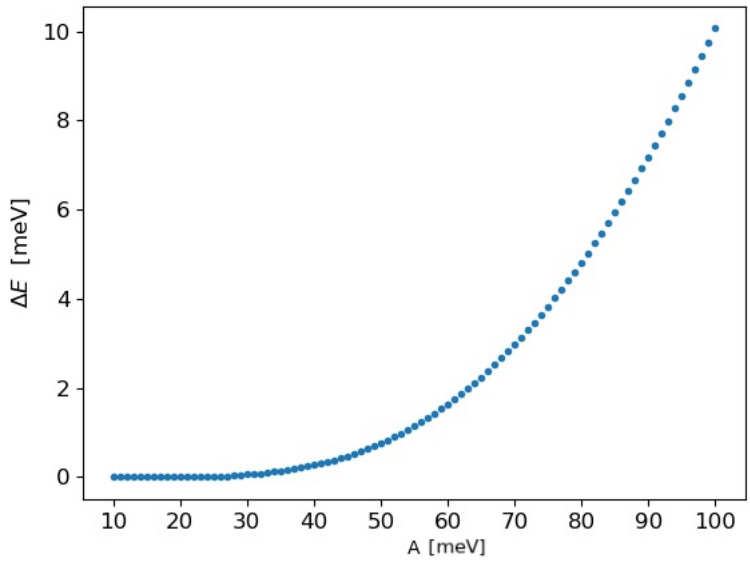

Figure 3.6: Valley splitting as a function of the strength of the parabolic confinement.

Chapter 4

Summary

In this thesis, we investigate the valley splitting in silicon quantum dots. We calculate the valley splitting in silicon and investigate the cases where different confining potentials are present.

First, we investigate the simplest tight-binding model which gives the correct result for the shape of the conduction band of silicon in 1D. After that, we use this model to calculate the valley splitting in a quantum well when we have an infinite potential well and parabolic confinement. In the first case, we test our numerical result with the analytical calculation done by Boykin *et al.* [31]. From our numerical simulation result, we observe an oscillation and a decaying trend in the valley splitting as we increase the number of sites in the square well potential.

In the second case, where we introduce parabolic confinement, we observe that the valley splitting increases as the strength of the parabolic confinement increases. When we set a low strength for this confinement, the valley splitting is on the same order of magnitude as in the case of a quantum well. However, the valley splitting will increase significantly as we set a higher strength for the parabolic confinement.

Acknowledgements

First of all, I would like to thank the almighty God for His mercy and blessing so I could finish this master thesis. I realize while completing this thesis, I also get much help from many people.

I would like to express my deepest gratitude to Dr. Széchenyi Gábor as my supervisor for his advice, guidance, and help during my research for this diploma project.

I also would like to thank the Ministry of Innovation and Technology (MIT) and the National Research, Development and Innovation Office (NKFIH) within the Quantum Information National Laboratory of Hungary for providing support for this project.

I am also grateful to my classmates for their help and willingness to spend their time in meaningful discussions. I am also thankful to my best friends for their genuine care especially through the hard times.

Finally, I would like to thank my dearest family, especially my parents, brothers, and sisters, for their endless motivation and support.

Bibliography

[1] Feynman, R. P. Simulating physics with computers. *Int. J. Theor. Phys.* **21**, 467-488, (1982).

[2] National Academies of Sciences, Engineering, and Medicine. *Quantum Computing: Progress and Prospects*. Washington, DC: The National Academies Press, (2019).

[3] L. K. Grover. A fast quantum mechanical algorithm for database search. *Proc. 28th Annual ACM Symposium on the Theory of Computing*, pp. 212-129, (1996).

[4] P. W. Shor. Algorithms for quantum computation: discrete logarithms and factoring. *Proceedings 35th Annual Symposium on Foundations of Computer Science*, pp. 124-134, (1994).

[5] Veldhorst, M. et al. An addressable quantum dot qubit with fault-tolerant fidelity. *Nature Nanotechnoly* **9** 981-985, (2014).

[6] Brown, K. R., Kim J, and Monroe C. Co-designing a scalable quantum computer with trapped atomic ions. *QuantumInformation* **2** 1-10, (2016).

[7] Arute, F., Arya, K., Babbush, R. et al. Quantum supremacy using a programmable superconducting processor. *Nature* **574**, 505-510, (2019).

[8] Arrazola J. M., V. Bergholm, K. Brádler, T. R. Brom-ley, M. J. Collins, I. Dhand, A. Fumagalli, T. Gerrits, A. Goussev, L. G. Helt, and et al. Quantum circuits with many photons on a programmable nanophotonic chip. *Nature* **591** 54-60. (2021).

[9] Chapman, Peter. Introducing the World's Most Powerful Quantum Computer. *IonQ*. Retrieved May 9, 2022, from https://ionq.com/posts/october-01-2020-introducing-most-powerful-quantum-computer

[10] Chow, J., Dial, O., Gambetta, J. IBM Quantum breaks the 100-qubit processor barrier. *IBM*. Retrieved May 9, 2022, from https://research.ibm.com/blog/127-qubit-quantum-processor-eagle

[11] Hendrickx NW, Lawrie WIL, Russ M, van Riggelen F, de Snoo SL, Schouten RN, Sammak A, Scappucci G, Veldhorst M. A four-qubit germanium quantum processor. *Nature*. **591**(7851):580-585. (2021).

[12] Ashoori R. C. Electrons in artificial atoms. *Nature* **379** 413, (1996).

[13] M. A. Reed. Quantum dots. *Scientific American* **268** 118, (1993).

[14] Kastner M. A. Artificial atoms. *Phys. Today* **46** 24, (1993).

[15] Hanson R, Awschalom DD. Coherent manipulation of single spins in semiconductors. *Nature*. **453** 1043, (2008).

[16] Hanson, R., Kouwenhoven, L. P., Petta, J. R., Tarucha, S. & Vandersypen, L. M. K. Spins in few-electron quantum dots. *Rev. Mod. Phys.* **79** 1217-1265, (2007).

[17] Prance, J. R., Z. Shi, C. B. Simmons, D. E. Savage, M. G. Lagally, L. R. Schreiber, L. M. K. Vandersypen, M. Friesen, R. Joynt, S. N. Coppersmith, and M. A. Eriksson. Single-Shot Measurement of Triplet-Singlet Relaxation in a Si/SiGe Double Quantum Dot. *Phys. Rev. Lett.* **108** (4), 46808, (2012).

[18] D. M. Zajac et al. Resonantly driven CNOT gate for electron spins. *Science* **359** 439, (2018).

[19] Nebel, C.E., Valleytronics: Electrons dance in diamond. *Nature Materials.* **12** (8):690-691, (2013).

[20] Rycerz, A., Tworzydło, J. & Beenakker, C. Valley filter and valley valve in graphene. *Nature Phys* **3**, 172-175, (2007).

[21] Shayegan, M., de Poortere, E. P., Gunawan, O., Shkolnikov, Y. P., Tutuc, E., Vakili, K. Two-dimensional electrons occupying multiple valleys in AlAs. *Physica Status Solidi (b).* **243** (14), 3629-3624, (2006).

[22] Sverdlov, V. *Strain-Induced Effects in Advanced MOSFETs*, ch. Basic Properties of the Silicon Lattice, pp. 35-44, Springer, Vienna, (2011).

[23] Zwanenburg, F.A., Dzurak, A.S., Morello, A., Simmons, M.Y., Hollenberg, L.C.L., Klimeck, G., Rogge, S., Coppersmith, S.N., Eriksson, M.A. Silicon quantum electronics. *Rev. Mod. Phys.* **85** 961-1019, (2013).

[24] Saraiva, A., Lim, W. H., Yang, C. H., Escott, C. C., Laucht, A., Dzurak, A. S., Materials for silicon quantum dots and their impact on electron spin qubits. *Adv. Funct. Mater.* **32**, 2105488, (2022).

[25] Morton, J., McCamey, D., Eriksson, M., and Lyon, S. Embracing the quantum limit in silicon computing. *Nature* **479**, 345-353, (2011).

[26] Bruzewicz, Colin D., Chiaverini, J.,McConnell, R., and Sage, Jeremy M. Trapped-ion quantum computing: Progress and challenges, *Applied Physics Reviews* **6**, 021314, (2019).

[27] Kane, B. A silicon-based nuclear spin quantum computer. *Nature* **393**, 133-137, (1998).

[28] Mi, X., Kohler, S., & Petta, J. R. Landau-Zener interferometry of valley-orbit states in Si/SiGe double quantum dots. *Physical Review B*, **98**(16), (2018).

[29] Culcer, D., Saraiva, A. L., Koiller, B., Hu, Xuedong, and Das Sarma, S. Valley-based noise-resistant quantum computation using Si quantum dots. *Phys. Rev. Lett.* **108**, 126804, (2012).

[30] Yang, C., Rossi, A., Ruskov, R. et al. Spin-valley lifetimes in a silicon quantum dot with tunable valley splitting. *Nat. Commun.* **4**, 2069, (2013).

[31] Boykin, T., G. Klimeck, M. Friesen, S. N. Coppersmith, P. Von Allmen, F. Oyafuso, and S. Lee. Valley splitting in low-density quantum-confined heterostructures studied using tight-binding models. *Phys. Rev. B* **70**, (2004).

[32] Hensel, J. C., Hasegawa, H., Nakayama, M. (1965). Cyclotron Resonance in Uniaxially Stressed Silicon. II. Nature of the Covalent Bond. Physical Review, 138(1A), A225–A238.

[33] P. C. W. Davies, and D. S. Betts. *Quantum Mechanics (Physics and Its Applications)*, ch. Wave mechanics 1, pp. 17-20, CRC Press, (1994).

List of Figures